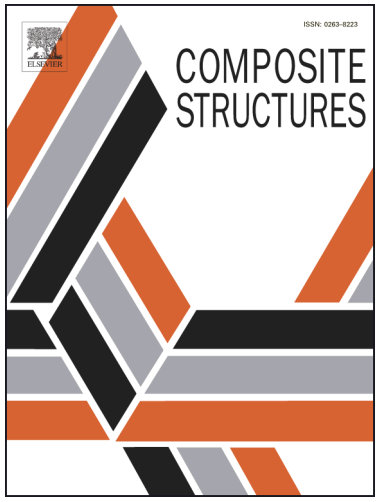

Lead-free piezocomposites with CNT-modified matrices: Accounting for agglomerations and molecular defects

A.K. Jagdish, Federico C. Buroni, Felipe Garcia-Sanchez, Roderick Melnik, Luis Rodriguez-Tembleque, Andres Saez

PII: S0263-8223(19)31320-0
DOI: https://doi.org/10.1016/j.compstruct.2019.111033
Article Number: 111033
Reference: COST 111033

To appear in: *Composite Structures*

Received Date: 12 April 2019
Accepted Date: 20 May 2019

Please cite this article as: Jagdish, A.K., Buroni, F.C., Garcia-Sanchez, F., Melnik, R., Rodriguez-Tembleque, L., Saez, A., Lead-free piezocomposites with CNT-modified matrices: Accounting for agglomerations and molecular defects, *Composite Structures* (2019), doi: https://doi.org/10.1016/j.compstruct.2019.111033

Lead-free piezocomposites with CNT-modified matrices: Accounting for agglomerations and molecular defects

A. K. Jagdish[1*], Federico C. Buroni[2], Felipe Garcia-Sanchez[3], Roderick Melnik[1,4], Luis Rodriguez-Tembleque[4], Andres Saez[4]

[1]MS2Discovery Interdisciplinary Research Institute, Wilfrid Laurier University, 75 University Ave W, Waterloo, Ontario, Canada, N2L 3C5

[2]Department of Mechanical Engineering and Manufacturing, Universidad de Sevilla, Camino de los Descubrimientos s/n, Seville E-41092, Spain

[3]Department of Civil Engineering, Materials, and Manufacturing, University of Malaga, Calle Dr. Ortiz Ramos s/n, 29071 Málaga, Spain

[4]Department of Continuum Mechanics and Structural Analysis, Universidad de Sevilla, Camino de los Descubrimientos s/n, Seville E-41092, Spain

Abstract: Piezoelectric matrix-inclusion composites based on lead-free ceramics have attracted attention due to the possibility of manufacturing environmentally friendly devices using scalable emerging technologies such as 3D printing. However, lead-free materials lag lead-based piezo-composites in terms of performance, thus necessitating new design strategies to escalate piezoelectric response. Here, we build a modeling paradigm for improving the piezoelectric performance through improved matrices and optimal polycrystallinity in the piezoelectric inclusions. By incorporating carbon nanotubes in the matrix, we demonstrate 2-3 orders of improvement in the piezoelectric response, through simultaneous hardening of the matrix and improvement in its permittivity. By tuning the polycrystallinity of the piezoelectric inclusions, we show considerable improvements exceeding 50% in the piezo-response, compared to single crystal inclusions. We further analyze the influence of carbon nanotube agglomerations at supramolecular length scales, as well as vacancy defects in the nanotubes at the atomic level, on composite performance. Although nanomaterial agglomeration is conventionally considered undesirable, we show that, near nanotube percolation, clustering of nanotubes can lead to better matrix hardening and higher permittivities, leading to improvements exceeding 30% in the piezoelectric response compared to non-agglomerated architectures. We further demonstrate that although atomic vacancy defects in nanotubes effectively soften the matrix, this can be compensated by agglomeration of nanotubes at larger length-scales.

Keywords: lead-free piezoelectric; composite; polycrystal; 3D printing; carbon nanotube; agglomeration; atomic defect; multiscale design and homogenization; coupled problems; finite element analysis; smart materials; network of contacts

1. Introduction

Piezoelectric composites represent an important class of materials which are frontrunners in integrated harvesting of ubiquitous mechanical energy. Specific applications can vary from wearable bio-mechanical energy harvesters [1-3] to application in civil infrastructure-integrated structural health monitoring devices [1, 4]. The interest in this class of materials stems from the possibility to tune the electro-elastic properties of the composite to suit application needs [1, 5]. A renewed interest in these material in the recent times is because of the possibility to manufacture them in a scalable manner using techniques such as 3D printing, which can lend microscale control over the fabrication process [5-8]. However, the performance of piezoelectric composites is limited by several factors. Firstly, this includes the relative softness of the matrix compared to the hard inclusions. The soft matrix takes up most of the applied strain and hence screens the inclusions from mechanical deformation, consequently reducing the piezoelectric response. Secondly, the matrices are typically polymeric, and hence have weak dielectric permittivity, compared to the poled inclusions. This prevents the electric flux generated within the inclusion from

*Corresponding author, email: ajagdish@wlu.ca

flowing freely within the composite and hence restricts the piezoelectric response. While these two common limitations (mechanical and electrical) are important, an additional factor that may strongly affect the performance of piezocomposites must be noted. Indeed, the polycrystalline microstructure of the inclusions also plays a critical role in determining the piezoelectric response of the composite [9, 10]. Although in isolation, polycrystals allow an enhanced piezoelectric response compared to single crystals, in composites, this behaviour is not apparent, mainly because of the electrical bottleneck discussed earlier [4, 11]. There is a growing need to develop novel design strategies to address these limitations, specially in the area of lead-free piezoelectric composites, which is the main motivation here. The need for efficient composite design is fuelled by two main reasons: (i) the need to develop lead-free materials for eco-friendly energy sensing/harvesting [1], and (ii) the need to enhance the performance of lead-free composites to the levels of lead-based composites, given a considerable current gap in their performances [1, 12]. The choice among lead-free piezoceramics is further constrained by the fact that a subset of these materials, such as Potassium-Sodium Niobate (KNN), pose considerable environmental threat in the process of extraction and disposal [13]. Therefore, in this paper, we focus on design strategies to enhance the performance of lead-free $BaTiO_3$-based composites and structures, which have attracted recent attention in the context of eco-friendly approaches to processing and fabrication [14, 15]. $BaTiO_3$-based composites have also been analyzed extensively through the development of models that study the nanoscale, microscale, and material dependent underpinnings of piezoelectric performance [16-24].

Here, we develop a modelling approach to simultaneously address these main limitations to piezoelectric composite performance, focusing on lead-free materials. In particular, we show that the elastic and dielectric properties of the matrix can be simultaneously improved by incorporating carbon nanotubes in the matrix. This becomes possible since carbon nanotubes simultaneously possess superior elastic properties, which can harden the matrix [25], and also excellent electrical conductivity, leading to percolative enhancement in dielectric permittivity of the modified matrix [26, 27]. While carbon-based nanomaterials, exemplified in this work by carbon nanotubes, are known to boost the piezoelectric response of composites [25], there are several important design issues that need to be addressed. One of the key such issues is connected with a low percolation threshold exhibited by nanotubes [27, 28], because of their high length-to-diameter aspect ratios and consequent ease with which percolative conducting networks are formed. This limits the amount of nanofiller that can be added to the matrix, and as a result, also limits the level of hardening in the matrix. Therefore, it is important to introduce material design variables which can help drive the percolation threshold up to higher values. It is well known that by reducing the aspect ratio of individual nanotubes, it is possible to increase the percolation threshold [27]. However, this comes at a cost of reduced matrix hardening [29], because higher aspect ratios are required for longer range fibrous reinforcement. On the other hand, we note that one of the aspects of composite design, which is traditionally considered undesirable, could possibly enable an increase in the percolation threshold, and hence in the piezoelectric response. In particular, more light should be shed on agglomeration of carbon nanotubes within the matrix, specifically in this context. Conventional composite designs aim at minimizing the percolation threshold and avoiding agglomeration [27, 30]. However, given the present requirements of increasing the percolation threshold, introducing controlled agglomerations could be a possible route to improve such conventional piezoelectric composite designs. This represents a design variation at the supramolecular level, which has recently generated interest in the literature due to enhanced electrical properties near percolation (e.g. [31]). Furthermore, at much smaller length scales, molecular/atomic defects such as vacancies also have an influence on the effective elastic properties of the nanotubes [32]. Therefore, this paper aims to bring in these novel aspects of design, stemming from atomic level variations to supramolecular clustering, to demonstrate their potential in tuning the electro-elastic properties of the matrix. Moreover, the model developed here will also consider practically viable, randomly shaped and randomly positioned polycrystalline piezoelectric inclusions. This is based on the observation that tuning the polycrystallinity can be an efficient strategy to improve the performance of lead-free piezoelectric ceramics and their composites [9, 11]. Based on the available experimental data and this model, we evaluate the piezoelectric enhancement in composites, through the introduction of

carbon nanotubes, by simultaneously hardening the matrix and improving its dielectric permittivity. In doing this, we create a design paradigm where the above aspects, across various length-scales, can be used to control the electro-elastic behaviour of the matrix, for achieving better composite performance.

The remainder of the paper is organized as follows: Section 2 provides the details of the model governing the coupled electro-elastic behaviour of the composite, along with the details of the composite geometry and boundary conditions. Section 3 provides details of the models describing the elastic and electrical properties of the constituent materials of the composite. In section 4, we discuss the role of supramolecular parameters (agglomeration), atomic defects (vacancies in CNTs), and their interplay in determining the piezoelectric performance of the composites. Section 5 summarizes our findings.

2. Composite geometry, coupled model, and boundary conditions

We study the steady state behaviour of a two-dimensional piezoelectric composite architecture consisting of microscale piezoelectric inclusions, carbon nanotubes and their agglomerates. The following sub-sections will provide details of the composite architecture, the coupled piezoelectric model used to study the behaviour of the composite, the materials models that govern the dielectric and mechanical properties of the composite, and the boundary conditions used to compute specific effective electro-elastic coefficients of interest.

2.1 Lead-free piezoelectric composites and geometric designs

We model the composite as a two-dimensional RVE in the x_1-x_3 plane as shown schematically in Figure 1. The composite is made of four components: (i) the rectangular matrix with dimensions a_m and b_m, (ii) microscale lead-free polycrystalline $BaTiO_3$ piezoelectric inclusions, which are randomly shaped and randomly positioned within the composite, (iii) non-agglomerated carbon nanotubes (multi-walled or single-walled), (iv) agglomerated bundles of carbon nanotubes (multi-walled or single-walled). Our analysis is exemplified for an RVE with dimensions a_m and b_m. The piezoelectric inclusions have dimensions of roughly 30 μm. More details on the geometry of the inclusions and the algorithm used to generate them are provided in appendix A1. The following considerations were taken into account while fixing the inclusion sizes: (i) the inclusions must be larger than the optimal grain sizes for enhanced piezoelectricity in polycrystals [10], which are in the sub-micron scale, and (ii) the inclusions must be larger compared to experimentally observed nanotube agglomerate sizes (≈3μm [33]), so that the matrix with stand-alone CNTs and agglomerated bundles of nanotubes can be treated as a homogeneous medium surrounding the inclusions. The carbon nanotubes considered here are either multiwalled ((15,15) MWCNTs) or single-walled ((15,15) SWCNTs). Based on the available experimental data, specifically in the case of the dielectric properties of carbon nanotube-modified polymeric matrices [30], we fix the nanotube aspect ratio $\lambda=L_{CNT}/2R_{CNT}$ at 100, where L_{CNT} and R_{CNT} are the length and the radius of the carbon nanotube. We summarize these geometrical parameters in Table 1.

2.2 Coupled electro-elastic fields of piezoelectric composites

The previous section provided the details of the composite geometry that is analysed in this paper. Here, we provide details of the electro-elastic model used to study the composite architecture detailed in section 2.1 and schematically shown in Figure 1. The basic relationships which linearly couple the electrical and mechanical fields are expressed as [11, 34]

$$\sigma_{ij}(\mathbf{x}) = c_{ijkl}(\mathbf{x})\varepsilon_{kl}(\mathbf{x}) - e_{ijk}(\mathbf{x})E_k(\mathbf{x}),\ D_j(\mathbf{x}) = e_{jkl}(\mathbf{x})\varepsilon_{kl}(\mathbf{x}) + \epsilon_{jk}(\mathbf{x})E_k(\mathbf{x}). \quad (1)$$

In (1) σ_{ij} and ε_{ij} are the components of the elastic stress and strain tensors, respectively, D_j are the components of the electric flux density vector, E_k are the components of the electric field vector, c_{ijkl}, e_{ijk}, and ϵ_{ij} are the elastic coefficients, piezoelectric coefficients, and the dielectric permittivity coefficients, and $\mathbf{x}$ is (x_1, x_3). The relationship between the strain field and the displacement vector, and the relationship between the electric field and the electric potential are respectively given by

$$\varepsilon_{ij} = \frac{1}{2}(u_{i,j}(\mathbf{x}) + u_{j,i}(\mathbf{x})), E_i(\mathbf{x}) = \ -\phi_{,i}(\mathbf{x}). \quad (2)$$

Considering the two-dimensional model discussed in Section 2.1, the equations (1)-(2) simplify into the following [11, 34]:

$$\vec{\boldsymbol{\sigma}} = \mathbf{C}\vec{\boldsymbol{\varepsilon}} - \mathbf{e}^T\vec{\mathbf{E}}, \ \vec{\mathbf{D}} = \mathbf{e}\vec{\boldsymbol{\varepsilon}} + \boldsymbol{\epsilon}\vec{\mathbf{E}}, \quad (3)$$

where $\vec{\boldsymbol{\sigma}} = (\sigma_{11} \ \sigma_{33} \ \sigma_{13})^T$, $\vec{\boldsymbol{\varepsilon}} = (\varepsilon_{11} \ \varepsilon_{33} \ \varepsilon_{13})^T$, $\vec{\mathbf{E}} = (E_1 \ E_3)^T$, and $\vec{\mathbf{D}} = (D_1 \ D_3)^T$. The matrices $\mathbf{C}$, $\mathbf{e}$, and $\boldsymbol{\epsilon}$ are defined as

$$\mathbf{C} = \begin{bmatrix} c_{11} & c_{13} & 0 \\ c_{13} & c_{33} & 0 \\ 0 & 0 & c_{44} \end{bmatrix}, \mathbf{e} = \begin{bmatrix} 0 & 0 & e_{15} \\ e_{31} & e_{33} & 0 \end{bmatrix}, \epsilon = \begin{bmatrix} \epsilon_{11} & 0 \\ 0 & \epsilon_{33} \end{bmatrix}. \quad (4)$$

These basic relationships are further subject to conditions of equilibrium and Gauss's law. Under the assumptions of vanishing body forces and vanishing volume charge densities, these governing equations are

$$\sigma_{ij,j}(\mathbf{x}) = \ 0, \ D_{i,i}(\mathbf{x}) = 0. \quad (5)$$

The phenomenological relationships given by equations (2)-(4), subject to the assumption-based governing relationships given by equation (5), determine the steady state behavior of a linear electro-elastic system. The well-posedness results in classes of generalized solutions for such coupled models, even in a more general dynamic setting, along with rigorous energy bounds, can be found in [35]. In our present analysis, this model has been implemented and simulated with the Finite Element Method in the context of the composite architecture specified in Figure 1.

2.3 Piezoelectric response of composites and boundary conditions

The previous sections provided the details of the composite geometry studied here and the coupled equations governing the piezoelectric behaviour of the composite. To evaluate the piezoelectric response of such composites, we calculate the effective e_{31} and e_{33} of the composite. The determination of these effective coefficients will need two separate boundary conditions which apply axial strains along the x_1 and x_3 directions [11, 34]. These are shown in Figure 2(a) and (b) and are further summarized in the appendix A1. Using boundary conditions BC1, we calculate the effective properties e_{11}^{eff}, c_{11}^{eff}, and c_{13}^{eff} of the composite. Using the second set of boundary conditions BC2, we calculate the effective properties e_{33}^{eff}, c_{33}^{eff}, and c_{13}^{eff} of the composite. In the following calculation, the volume average of a quantity A is represented as $\langle A \rangle$ and is calculated as

$$\langle A \rangle = \frac{1}{a_m b_m}\int_\Omega A d\Omega, \quad (6)$$

where Ω is the volume over which the integration is carried out, which in this case is the total volume of the RVE.

By applying the boundary conditions BC1, the following volume averages are obtained,

$$\langle \varepsilon_{11} \rangle = \overline{\varepsilon_{11}} \quad , \quad \langle \varepsilon_{33} \rangle = \ 0, \quad \langle \varepsilon_{13} \rangle = \ 0, \quad \langle E_i \rangle = 0. \quad (7)$$

Using these volume averages, the following effective coefficients of the composite are calculated as [11, 34]

$$e_{31}^{eff} = \frac{\langle D_3 \rangle}{\overline{\varepsilon_{11}}}\ ,\ c_{11}^{eff} = \frac{\langle \sigma_{11} \rangle}{\overline{\varepsilon_{11}}}\ , c_{13}^{eff} = \frac{\langle \sigma_{33} \rangle}{\overline{\varepsilon_{11}}}, \tag{8}$$

where $\langle D_3 \rangle$ is the volume average of the D_3 component of the electric flux density vector. Similarly, by using the second set of boundary conditions BC2, the following set of volume averages are obtained

$$\langle \varepsilon_{11} \rangle = 0\ , \langle \varepsilon_{33} \rangle = \overline{\varepsilon_{33}}, \langle \varepsilon_{13} \rangle = 0\ , \langle E_i \rangle = 0. \tag{9}$$

These volume averages are further used to calculate the following effective coefficients of the composite.

$$e_{33}^{eff} = \frac{\langle D_3 \rangle}{\overline{\varepsilon_{33}}}\ , c_{33}^{eff} = \frac{\langle \sigma_{33} \rangle}{\overline{\varepsilon_{33}}}, c_{13}^{eff} = \frac{\langle \sigma_{11} \rangle}{\overline{\varepsilon_{33}}}. \tag{10}$$

In our calculations, we assume small strains and accordingly set $\overline{\varepsilon_{11}}$ and $\overline{\varepsilon_{33}}$ in BC1 and BC2, respectively, to 1×10^{-6}.

3. Material Models, CNT additions, and polycrystalline piezoelectric inclusions

In this section, we provide details of the models and experimental data that describe the electro-elastic properties of the non-piezoelectric PDMS matrix, the polycrystalline $BaTiO_3$ inclusions, and the carbon nanotubes that are added to the matrix.

3.1 Matrix models

We choose a soft polymer matrix, polydimethylsiloxane (PDMS), for our analysis. Experimental efforts to fabricate piezoelectric composites with soft matrices, by using 3D printing and other emerging technologies, have been receiving an increasing attention in literature [8, 15]. However, such soft matrices pose a dual challenge. First, their soft elastic properties screen the applied mechanical stimuli from the $BaTiO_3$, thus resulting in a very small electric flux generation. Secondly, polymeric materials, in general, are weak dielectrics and thus impede the flow of electric flux out of the piezoelectric inclusions. However, a number of experiments, including recent efforts in these directions, indicate that both of the above issues can be circumvented. In particular, soft polymeric matrices can be hardened significantly by the addition of very small quantities of carbon nanotubes [25], with a simultaneous enhancement in the effective dielectric permittivity [26]. On the basis of these experimental observations, a soft matrix, exemplified here by PDMS, forms an ideal candidate to evaluate the possible improvements in the piezoelectric response, through elastic and dielectric enhancements.

The elastic coefficients of the matrix are obtained from its Young's modulus E_m and its Poisson's ratio ν_m , as described by equations (11)-(12) below:

$$\mathbf{C_m} = \begin{bmatrix} \lambda_m + 2\mu_m & \lambda_m & \lambda_m & 0 & 0 & 0 \\ \lambda_m & \lambda_m + 2\mu_m & \lambda_m & 0 & 0 & 0 \\ \lambda_m & \lambda_m & \lambda_m + 2\mu_m & 0 & 0 & 0 \\ 0 & 0 & 0 & \mu_m & 0 & 0 \\ 0 & 0 & 0 & 0 & \mu_m & 0 \\ 0 & 0 & 0 & 0 & 0 & \mu_m \end{bmatrix}, \tag{11}$$

where

$$\lambda_m = \frac{E_m \nu_m}{(1+\nu_m)(1-2\nu_m)} \quad , \quad \mu_m = \frac{E_m}{2(1+\nu_m)} \quad . \tag{12}$$

Table 2 summarizes the material constants of the PDMS matrix for which computations have been carried out. The addition of carbon nanotubes and their agglomerates will further modify E_m and ν_m.

The effective elastic moduli of the CNT-modified matrix are obtained by using a two-parameter model, which calculates the effective properties based on the elastic coefficients of the pristine matrix, summarized in Table 2. Thermal degradation and thermal stability analysis of PDMS-based polymeric composites is an important issue that lies outside of the scope of this paper. We note, however, that a computationally efficient procedure for such analysis, developed for polymeric materials in a generic setting [36], can be incorporated in our modelling framework. We also refer the interested reader to several experimental works in this direction [37-39]. It is notable, from these works, that there is growing experimental evidence that the incorporation of CNTs may significantly enhance the thermal stability of composites, including those which are in the center of our attention here.

In our examples reported in section 4, the matrix is modified by addition of (15,15) multiwalled carbon nanotubes (MWCNTs) and single-walled nanotubes (SWCNTs). Our analysis of agglomeration of nanotubes is based on the addition of MWCNTs and the analysis of atomic scale vacancies is based on that of SWCNTs, where the presence of vacancies is expected to have a more considerable effect on the elastic properties of the nanotube. This alters both the elastic and the dielectric properties of the matrix. Firstly, addition of nanotubes hardens the matrix, thus leading to higher Young's moduli (Figure 3(a), in the case of (15,15) MWCNTs). This is also accompanied by a reduction in the Poisson's ratio (Figure 3(b), in the case of (15,15) MWCNTs). This hardening is also affected by agglomeration of nanotubes. By using the transversely isotropic elastic properties of carbon nanotubes [41] and the elastic properties of the pristine matrix (cf. Table 2), the effective Young's modulus and Poisson's ratio of the matrix are modelled with a two-parameter model [41-43]. The model takes into account the agglomerations of the nanotubes through two parameters ξ and ζ. While the latter is the fraction of the nanotubes, in the matrix, that are agglomerated, the former is the volume fraction of the agglomerates in the composite matrix. When the parameters are equal, there are no agglomerations and CNTs are dispersed uniformly in the matrix. When $\xi < \zeta$, there are agglomerates. We consider two representative cases: $\xi = \zeta$ and $\xi = 0.5\zeta$. The variation of the effective Young's modulus E_m^{eff} and the Poisson's ratio ν_m^{eff} of the matrix, as a function of volume fraction f_{CNT} of MWCNTs are shown in Figure 3(c)-(d), respectively, for these two states of agglomeration. It is seen that the hardening of the matrix is reduced (Figure 3(c)) in the presence of the agglomerates and the effective Poisson's ratio is higher in the matrix with agglomerates (Figure 3(d)). Further, the introduction of atomic vacancy defects in the nanotubes brings about a reduced effective Young's modulus and an increased Poisson's ratio in the matrix, as shown in Figures 3(e)-(f), for (15,15) SWCNT-modified matrices. Therefore, from the perspective of the effective elastic properties of the matrices, it appears that nanotube-agglomeration and atomic defects adversely affect the matrix hardening with CNTs, thus pointing to a reduced enhancement in the piezoelectric response.

The addition of MWCNTs also increases the dielectric permittivity of the matrix. Based on existing experimental evidence [27, 44], the variation of the dielectric constant with f_{CNT} follows a percolation behaviour, described by the equation

$$\epsilon_m^{eff} = \epsilon_m \left(\frac{f_c}{f_c - f_{CNT}} \right)^p, \tag{13}$$

where ϵ_m is the relative permittivity of the pristine polymer matrix, f_c is the percolation threshold of the nanotubes, f_{CNT} is the volume fraction of the nanotubes in the matrix, and p is a critical exponent determining the percolative variation of the effective permittivity. The percolation threshold, f_c, and the critical exponent, p, are functions of mainly the aspect ratio of the MWCNTs and the agglomeration characteristics. Experiments clearly show that when the aspect ratio of the CNTs is unchanged, agglomeration of the nanotubes leads to an increased percolation threshold [27, 30]. Intuitively, this means that for a given volume fraction V_{CNT} of nanotubes in the composite, agglomeration reduces the probability of establishing a connected network, and hence increases the percolation threshold. Several models have been developed to understand the dependence of the agglomeration state of a composite and its percolation threshold (e.g. [27, 30]). We apply here a model developed in [30] which expresses the

agglomeration state of the system using the parameter ζ, which is the fraction of the total number of nanotubes that are agglomerated. This model estimates ζ for various experimental samples, using the observed values of f_c. However, this estimation assumes that all agglomerates consist of 7 CNTs which are hexagonally close-packed [45]. The validity of this approach is discussed further and generalized in Appendix A2. As it stands now, to the best of our knowledge, this is the most complete experimental data currently available, which analyses CNTs of similar aspect ratios across different agglomeration states. Therefore, it is expected that this model can provide a revealing critical insight into the role of agglomeration in deciding the effective dielectric properties of the matrix. Using this model, the analytical relation [30] between f_c and ζ is expressed as

$$f_c = \frac{m\zeta(1+S_1)(1+S_2)(3\lambda+2) + (1-\zeta)(1+S_1)(1+S_2)(3n^2\lambda+2n^3)}{2m\zeta(1+S_2)(3\lambda^2+12\lambda+8) + 2(1-\zeta)(1+S_1)(3n\lambda^2+12n^2\lambda+8n^3)}, \quad (14)$$

where m is the number of CNTs in an agglomerate, n is a factor multiplying the radius R_{CNT} (refer to Table 1) of the nanotube to give an approximate radius of the agglomerate, $S_1 = 5.231(2\lambda)^{-0.569}$, and $S_2 = 5.231n^{0.569}(2\lambda)^{-0.569}$.

Table 3 lists the calculated parameter ζ for various experimentally measured values of f_c, when carbon nanotubes with aspect ratio of $\lambda = 100$ are dispersed in varying agglomeration states, in a polymer matrix. It is seen, that as the fraction ζ of agglomerated MWNCTs increases, the percolation threshold also increases. From equation (14), we also calculate predicted percolation threshold for a sample with no agglomerations (i.e. $\zeta = 0$), which is equal to 0.608%.

There is no conclusive evidence in the literature on the value of critical exponent. However, it has been demonstrated that by chemical functionalization of nanotubes, the critical exponent, p, can be tuned in the range 1.0-1.23 [46]. Smaller values of p, nearing 0.8, have also been reported [47]. We therefore assume p=1.2 in our analysis which allows the best dielectric enhancement, on the basis of experimental observations. Figure 4 shows an example plot of ϵ_m^{eff} for f_c=1.0 and p=1.2.

3.2 Polycrystalline model for piezoelectric inclusions

We consider polycrystalline piezoelectric inclusions, where the electro-elastic coefficients depend on the polycrystalline microstructure. The motivation to consider polycrystals in piezoelectric composites stems from recent findings, where it was demonstrated that inclusions with controlled randomness in domain/grain-orientation can outperform single crystalline inclusions, provided the matrix has a high permittivity, which is capable of efficiently coupling electric flux through the composite [4, 11]. Furthermore, the interest to consider polycrystalline inclusions is driven by the fact that lead-free materials such as $BaTiO_3$, which form the central aspect of this paper, are shown to exhibit better piezoelectric performance compared to their single crystal counterparts [9]. The basis of our consideration has been the model developed in [9] to obtain the effective properties of polycrystalline inclusions as a function of parameter α, which quantifies the orientation of the poled polycrystal. When α tends to zero, the polycrystal is highly oriented and resembles a single crystalline inclusion. On the other extreme, when α tends to infinity, we have a highly disoriented polycrystal with no net piezoelectric activity. The model and the effective electro-elastic coefficients are summarized in the appendix A3. We emphasize here that the parameter α can be tuned by controlling the poling process – the poling electric field, temperature and so on, for which different experimental techniques exist [48]. However, exact experimental measurements of α is still a challenge.

4 Results and discussion

We divide our discussion into three sections. First, we will discuss the effects of incorporating well dispersed, non-agglomerated, (15,15) MWCNTs in the matrix, on the piezoelectrtic performance. This

will be followed by a discussion of our findings on the influence of agglomerated clusters of CNTs in the analysis of piezoelectric response. Thirdly, we will consider the effects of atomic vacancy defects on the piezoelectric performance. Our study has been exemplified here for 5 different RVEs with increasing volume fractions V_p of the piezoelectric inclusions, as shown in Figure 5.

4.1 Piezoelectric composites with non-agglomerated nanotubes

Incorporation of carbon nanotubes has a dual effect – hardening of the matrix and improving its dielectric constant. These two aspects can act synergistically to improve the piezoelectric response relative to the composite without nanotubes. In our simulations for this study involving non-agglomerated nanotubes, we fix f_c=1.0 and p=1.2 which are close to experimentally observed values as discussed in section 3.1. First, we notice that as the nanotube volume fraction f_{CNT} increases, the effective elastic moduli of the matrix also increase, as shown in Figure 6, for α=0 and for several representative volume fractions V_p of piezoelectric inclusions. It is seen that the polycrystallinity of the piezoelectric inclusions has little effect on the effective elastic moduli, compared to the more pronounced effect of the nanotube fill-fraction. Furthermore, the introduction of carbon nanotubes enhances the permittivity of the matrix, following a percolative behaviour. In the vicinity of the percolation threshold, the effective permittivity of the matrix dramatically increases, as shown by Figure 4. Such high permittivities allow a relatively easy flow of electric flux from the piezoelectric inclusions [4, 11], leading to better piezoelectric performance.

Owing to the large elastic moduli of the piezoelectric inclusions, the effective moduli also increase as V_p increases. However, the key point is that for a given V_p, the inclusion of nanotubes in the matrix leads to an almost linearly dependent increase in the elastic moduli of the composite. The increased hardness of the matrix can now efficiently channel the applied mechanical stimuli to the piezoelectric inclusions, which otherwise would have been screened. In fact, by breaking the electrical bottleneck imposed by the otherwise weak-dielectric environment, composites with polycrystalline piezoelectric inclusions having controlled random domain orientations (dictated by the parameter α), exhibit better piezoelectric behaviour. This behaviour is seen in the plots of the effective parameters e_{31} and e_{33} of the composites, irrespective of V_p (Figures 7(a)-(e) and 8(a)-(e)). The combined effect of matrix hardening and dielectric enhancement in the matrix leads to considerable improvements in both the effective piezoelectric coefficients. This shows that the inclusion of nanotubes in piezoelectric composites, and in particular in lead-free materials analyzed here, is a viable design strategy for significant improvements in piezoelectric performance. Further, from Figures 7(f) and 8(f), we notice that the enhancement in the effective piezoelectric coefficients of polycrystalline-inclusion-based composites is higher for higher inclusion volume fractions V_p. This is because of better electrical coupling between the high permittivity inclusions, when they are relatively closer to each other. In the case of the RVE with V_p=43.16%, we notice almost a 50% improvement in the effective coefficients e_{31} and e_{33}, around α=0.5, compared to the values of the single-crystal-based composite (α=0). We further analyze the variation in the effective piezoelectric coefficients e_{31} and e_{33} of the composites, for different V_p, as a function of the nanotube fill-fraction f_{CNT} (Figure 9). Here, we study the behaviour of the composites with $\alpha = 0.5$, which from our preceding analysis, represents an optimal polycrystalline configuration for the piezoelectric inclusions. From Figure 9(a)-(b), it is clear that the effective piezoelectric coefficients improve with increasing CNT addition, with the curves suggesting a percolative behaviour. Figures 9(c)-(d) further show the effective coefficients e_{31} and e_{33}, respectively, relative to their values with no CNT additions. These figures reveal that addition of CNTs can lead to improvements exceeding 2-3 orders of magnitude in both the effective coefficients. The negative sign in Figure 9(c) indicates the reversal of the sign of the effective e_{31}, which is positive for a pristine matrix and negative for a CNT-modified matrix. This sign reversal follows from the reduction in the Poisson's ratio of the matrix on addition of CNTs, as seen in Figure 3(b), which causes a reversal in the direction of the strain component ε_{31} [11]. This demonstrates that soft polymeric matrices modified

with carbon nanotubes and piezoelectric inclusions, which are poled to obtain optimal randomness in domain orientation (optimal α), can exhibit significantly higher piezoelectric performances.

4.2 Piezoelectric composites with partially agglomerated nanotubes

We have seen that well-dispersed nanotubes lead to significant improvements in the piezoelectric response. However, in the experimental scenario, it is common for nanotubes to get agglomerated, because of varying processing conditions [27]. Further, the degree of agglomeration of nanotubes within a composite can be controlled by tuning the process parameters. Therefore, controlled agglomeration can be viewed as a material design parameter, which would allow the tuning of the effective mechanical and electrical properties of the composite. With respect to f_{CNT}, the fill-fraction of the nanotubes, we consider two cases for our analysis: (i) the behaviour where f_{CNT} is not large enough for the matrix to achieve high permittivities due to percolative enhancement (in particular, we consider f_{CNT}=0.5%), and (ii) the behaviour just before percolation (in particular, we consider f_{CNT}=0.999f_c). Our representative example will be shown for the composite architecture with 16 inclusions (V_p=26.67%).

Figures 10(a) and (b) show the effective coefficients e_{31} and e_{33} of the composite, as a function of α when f_{CNT}=0.5%. It is clear from these plots, that the agglomeration of nanotubes has a detrimental effect on the piezoelectric response. This is because, agglomeration leads to lesser matrix-hardening compared to the well-dispersed matrix architecture (Figure 3(c)). Although agglomeration leads to an increased percolation threshold, and consequently to a higher matrix permittivity (cf. Formula (13)), this increase is opposed by a reduction in the effective elastic moduli of the matrix due to agglomeration. Therefore, when the nanotube fill-fractions are substantially smaller than the percolation threshold, agglomeration of nanotubes is undesirable. However, at percolation, the situation reverses. Agglomeration leads to increased percolation thresholds, thus allowing the addition of higher nanotube content in the matrix before percolation. Moreover, although agglomeration of nanotubes reduces the hardening effect, this can eventually be compensated with the addition of more nanotubes into the matrix because of a larger window before percolation. Hence, at percolation, it is seen that the matrices with agglomerated nanotubes are harder than the matrices with well-dispersed nanotubes, at the cost of higher amounts of CNT additions. Also, at percolation, the permittivities of the matrices escalate to large values, with the agglomerated architecture exhibiting higher permittivities. Under such conditions, the mechanical hardening of the matrix and the dielectric enhancement through percolation contribute synergistically towards an improved piezoelectric response. As seen from Figures 10(c) and (d), at nanotube percolation, agglomeration leads to better effective coefficients e_{31} and e_{33} compared to composites with non-agglomerated matrices. It is further seen that higher agglomerations (higher ζ) can lead to better piezoelectric response. Thus, the agglomeration of nanomaterial fillers, which is conventionally seen to be detrimental to composite performance, could also be desirable, at least to some extent, in the context of enhanced piezoelectric composite performance. Taking into account the experimental data considered here, for the agglomerations, the improvements in both the effective coefficients, e_{31} and e_{33}, exceed 30% (Figure 10(c)-(d)). There is further scope for improvement in the piezoelectric performance through optimal agglomeration engineering. In achieving this goal, our current analysis may complement and provide further insight to the development of advanced molecular modelling and experimental techniques for polymeric composites [49-54]. At the same time, this analysis is attainable on scales substantially larger than more refined atomistic and molecular modelling methodologies would presently allow, which is a critically important feature for emerging scalable technologies such as 3D printing.

To summarize this part of the study, we notice that the agglomeration of nanotubes has two competing effects on the piezoelectric performance. Firstly, agglomeration reduces the hardening of the matrix compared to well-dispersed composite architectures. This reduces the piezoelectric activity, away from the percolation threshold of nanotubes. However, because of the increased percolation thresholds in matrices with agglomeration, and a consequent larger allowance to introduce more nanomaterial before percolation occurs, the agglomeration process may lead to both better hardening and higher matrix

permittivities, near percolation, compared to well-dispersed matrices. Therefore, matrices with adequately dispersed carbon nanotubes with a small amount of remnant agglomeration might be optimal for enhanced piezoelectric performance of the composite.

4.3 Piezoelectric composites modified by carbon nanotubes with atomic vacancy defects

We now consider the effects of atomic scale defects, such as vacancy defects, on the piezoelectric response of the composite. Molecular simulations have provided evidence that both the Young's modulus and the Poisson's ratio of carbon nanotubes decrease on the introduction of even a small amount of vacancies (vacancy concentration f_v=1-2%) [32]. This removal of atoms from their lattice positions softens the nanotubes, and in the context of piezoelectric composites, this means that the hardening effect of the carbon nanotubes on the matrix will be reduced. Having this in mind, in this section we consider the possibility of using a supramolecular effect of CNT-agglomeration to negate the influence of molecular-scale defects. In particular, we consider for our analysis (15,15) single-walled carbon nanotubes, because in this case the effect of vacancy defects is expected to be more pronounced than in MWCNTs. We assume the same percolation thresholds, as those of MWCNTs. Figures 11(a)-(c) show the effective Young's modulus of the matrix in the presence of defective and agglomerated nanotubes, for various defect concentrations f_v and agglomeration states (in the range of interest for this analysis). Similarly, Figures 11(d)-(f) show the effective Poisson's ratio of these matrices. Only small vacancy concentrations (1-2%) are considered and two agglomeration states corresponding to $\zeta = 0.15, \xi = 0.5\zeta$ and $\zeta = 0.40, \xi = 0.5\zeta$ are analyzed. The reference composite architecture for comparison in all these cases has no agglomerations (i.e. $\zeta = \xi$) and no vacancy defects (f_v=0%). We scrutinize the behaviour of the composite near nanotube percolation. Away from percolation, the implications of defects and agglomerations are trivial in that they would lead to a reduced piezoelectric response. Figures 12(a)-(b) show the effective parameter e_{31} of the composite, as a function of α, for vacancy concentration f_v =1% and 2% respectively. Figures 12(c)-(d) show similar results for the effective parameter e_{33} of the composites. It is seen from these results that in the composites with no nanotube agglomerates, an increase in the vacancy concentration f_v results in decreased effective coefficients e_{31} and e_{33}. However, with the introduction of agglomerates, the situation improves, because of the increased percolation threshold and the consequently widened window for CNT-addition. As the degree of agglomeration increases (i.e. as ζ increases), the piezoelectric response of the structures with atomic defects improves beyond the reference composite architecture which has neither agglomerates nor atomic defects. Further, on comparing the results for f_v=1% and 2%, it is evident that as the vacancy concentration increases, more agglomerations would be needed to compensate the influence of atomic defects. Therefore, the loss in the matrix-hardening due to defective nanotubes can be compensated by nanotube agglomerations. This opens up new design paradigms where the degradation of a material property at atomic scales can be compensated by constructive material design at a larger length scale.

5 Conclusions

In summary, we have devised a computational framework to analyse enhanced piezoelectric composite designs through the inclusion of mechanically and electrically superior carbon nanotubes in the matrix. In particular, we have observed that carbon nanotubes can simultaneously harden the matrix and improve its dielectric constant resulting in considerable improvements in the piezoelectric response that may exceed 2-3 orders of magnitude. Such improvements are further increased together with the increase in the volume fractions of the piezoelectric inclusions. The performance of composites with polycrystalline piezoelectric inclusions with optimally tuned randomness in their domain orientations can exceed the performance of their single-crystal counterpart composite designs by up to 50%, at carbon nanotube percolation conditions. Further, we have also demonstrated that agglomeration of carbon nanotubes, which is often considered undesirable, can help enhance piezoelectric performance under certain conditions. While the agglomeration reduces the extent of hardening in the matrix, it also increases the percolation threshold, which allows for addition of more nanotubes and further hardening. Therefore, at

percolation, the matrix is both harder and has higher permittivity compared to matrices at percolation without agglomerates. This leads to a higher piezoelectric response, at percolation, in composites which have carbon nanotube agglomerates. With the agglomeration states considered in our study, we predict improvements exceeding 30% in the effective piezoelectric coefficients. This improvement can be further tuned through optimal engineering of nanotube agglomerations. Finally, we considered the influence of atomic scale vacancy defects in the CNT on the performance of the composites. Although atomic vacancies soften the nanotubes and thus impede matrix-hardening, this can be compensated through the introduction of constructive molecular design at larger length scales, in the form of nanotube agglomerations. Through increased percolation thresholds, composites with agglomerated and defective CNTs are demonstrated to perform better in comparison to composites without agglomerates and atomic defects. Therefore, this work opens up new design paradigms in which conventionally undesirable material properties at atomic and supra-molecular length scales can be simultaneously engineered to improve the performance of piezoelectric composites.

Acknowledgments

This work was supported by the Ministerio de Economía y Competitividad of Spain and the European Regional Development Fund under projects DPI2014-53947-R and DPI2017-89162-R. RM and AKJ are also grateful to the NSERC and CRC program for their support. Authors thank the colleagues from the Soil, Structures and Materials Mechanics Laboratory (MSSMat) at UMR CNRS in France, in particular Dr.Benhui Fan, for a useful discussion pertaining to PDMS/CNT composites and for providing raw experimental data for the effective dielectric properties of the composite matrix.

Appendices

A1: Randomly shaped polycrystalline inclusions and boundary conditions: computational implementation

The random shapes were generated using a MATLAB code. The algorithm for the generation of the random shapes is summarized below

Step 1 – Select a random number of sides n for the polygon to be generated in the range $[n_1, n_2]$.

Step 2 – Select random angle θ_0 between 0° and 90°. Select the range of random radii R_1 and R_2 defining the concentric circles within which the random shape will be spatially bounded. The center of these circles is the origin of the local coordinate system.

Step 3 - Select an initial R_0 in the range $[R_{min}, R_{max}]$. The first vertex of the random object is defined in the local coordinates as (R_1, θ_1), where the reference origin is at the center of the random concentric circles.

Step 4 – The next vertex of the polygon is at (R_2, θ_2) (in general (R_i, θ_i)) in the local coordinate system, which is obtained by a random incremental rotation by an angle θ, about the local origin, which is in the range $[10°, \theta_{max} = 360/n]$, and a random selection of the radius R in the range $[R_1, R_2]$. Joining the points (R_{i-1}, θ_{i-1}) and (R_i, θ_i) by a straight line, to form the i^{th} edge of the polygon

Step 5 – Repeat Step 4 till the total rotation adds up to 360°. Now there are "n+1" sets of coordinates. It is to be ensured that $(R_0, \theta_0) = (R_n, \theta_n)$. Join these points by a straight line to get the n^{th} edge of the polygon

Parameters used in the study:

For each inclusion, the number of sides, n, of the polygonal inclusion, is chosen in step one, randomly in the range $[n_1, n_2]$, where

n_1: 10

n_2: 20

Also, the two bounding concentric circles within which the inclusion is spatially bounded, have radii R_1 and R_2 which are randomly selected as follows:

R_1: Randomly chosen between 7.5 μm and 10.5 μm.

R_2: Randomly chosen between 12 μm and 15 μm.

This algorithm generates polycrystals of sizes not exceeding 30 μm. i.e. the inclusions are spatially bounded within concentric circles of average radii 9 μm and 13.5 μm.

There are two boundary conditions used in the calculations – BC1 and BC2 as highlighted schematically in Figure 2. The two boundary conditions and the corresponding effective parameters of the composite which are calculated through its application are listed below:

1) BC1 – c_{11}^{eff}, c_{13}^{eff},e_{31}^{eff}
2) BC2 - c_{33}^{eff}, c_{13}^{eff},e_{33}^{eff}

The computations were carried out with minimum and maximum element sizes of 10 nm and 2 μm, respectively. Convergence was achieved with mesh refinements which were carried out to resolve the sharp regions of transitions around the random edges and vertices of the randomly shaped inclusions.

A2: The validity of the analytical relation between the percolation threshold and agglomeration state

Equation (14), originally derived in [30], expressed analytically the relationship between the percolation threshold for CNTs in a matrix and the fraction ζ of the total nanotubes that are agglomerated. We note that the calculations in [30] assume that the all agglomerates are a bundle of 7 carbon-nanotubes, hexagonally close-packed. This is a restrictive assumption in many practical scenarios where the agglomerate size can be random. We modify equation (14), by considering a more general relationship between m and n. Equation (14) is given below for convenience and clarity of the arguments that follow.

$$f_c = \frac{m\zeta(1+S_1)(1+S_2)(3\lambda+2)+(1-\zeta)(1+S_1)(1+S_2)(3n^2\lambda+2n^3)}{2m\zeta(1+S_2)(3\lambda^2+12\lambda+8)+2(1-\zeta)(1+S_1)(3n\lambda^2+12n^2\lambda+8n^3)}.$$

(AE1)

By using available geometrical data for the number of non-intersecting smaller circles that can be packed within a larger circle[AR], we derive following relation between n and m:

$$n = 0.8179\log(m) + 0.08226m + 1.02$$

(AE2)

By combining equations (AE1) and (AE2), we obtain a more general relation between f_c and ζ. Taking the experimentally measured percolation thresholds from [30] (cf. Table 3), we calculate ζ, using the above relations. The results are plotted in Figure AF1. It is seen that when only a small portion of CNTs are agglomerated, for agglomerates having more than approximately 5 CNTs, ζ depends only weakly on m, and could be considered constant in a first order approximation. Hence, the assumption made in [30] could be justifiable even in real scenarios where agglomerate sizes are random. It should be noted that in the composites with higher percolation thresholds, where a larger portion of the CNTs are agglomerated, the dependence of ζ on m is stronger. Therefore, a simplistic model which assumes that agglomerates are of constant sizes, provides a less realistic picture as the agglomeration density increases. To develop our

[AR] Friedman, E., Circles in circles, 2005, https://www2.stetson.edu/~efriedma/cirincir/ (Date accessed 19 March 2019)

arguments even further, more sophisticated multiscale models, accounting for molecular interactions and random agglomeration sizes, would be necessary. Moreover, for random agglomeration packing densities, it would be necessary to obtain more accurate relations between the random composite structure and the percolation threshold, which require further experimental work in this area.

A3: The effective electro-elastic coefficients of polycrystalline $BaTiO_3$ piezoelectric inclusions

The effective elastic, piezoelectric, and relative permittivity coefficients of polycrystalline $BaTiO_3$ were obtained, by interpolation, from [9]. These effective properties are plotted in Figure AF2. As explained in the main text, these coefficients are functions of orientation parameter α which can vary from 0 to ∞. $\alpha \to 0$ corresponds to a single-crystal or a polycrystal with all grains having similar orientation. The other extreme $\alpha \to \infty$ corresponds to a randomly oriented polycrystal, in which there is no net piezoelectric activity. It is notable that, in isolated polycrystals of $BaTiO_3$ (with $\alpha \approx 0.5$), the effective coefficients e_{33} and e_{31} exhibit higher values compared to highly oriented crystals, which we exploit in a composite architecture by using matrices with enhanced permittivities.

References

[1] Maurya D, Peddigari M, Kang M-G, Geng L D, Sharpes N, Annapureddy V, Palneedi H, Sriramdas R, Yan Y and Song H-C 2018 Lead-free piezoelectric materials and composites for high power density energy harvesting *Journal of Materials Research* **33** 2235-63

[2] Lee M, Chen C Y, Wang S, Cha S N, Park Y J, Kim J M, Chou L J and Wang Z L 2012 A hybrid piezoelectric structure for wearable nanogenerators *Advanced Materials* **24** 1759-64

[3] González J L, Rubio A and Moll F 2002 Human powered piezoelectric batteries to supply power to wearable electronic devices *International journal of the Society of Materials Engineering for Resources* **10** 34-40

[4] Li Z, Zhang D and Wu K 2002 Cement-Based 0-3 Piezoelectric Composites *Journal of the American Ceramic Society* **85** 305-13

[5] Phatharapeetranun N, Ksapabutr B, Marani D, Bowen J R and Esposito V 2017 3D-printed barium titanate/poly-(vinylidene fluoride) nano-hybrids with anisotropic dielectric properties *Journal of Materials Chemistry C* **5** 12430-40

[6] Agnelli F, Constantinescu A and Nika G 2018 Optimal design of auxetic, additively manufactured, polymeric structures *arXiv preprint arXiv:1809.02467*

[7] Kim H, Torres F, Villagran D, Stewart C, Lin Y and Tseng T L B 2017 3D printing of BaTiO3/PVDF composites with electric in situ poling for pressure sensor applications *Macromolecular Materials and Engineering* **302** 1700229

[8] Kim K, Zhu W, Qu X, Aaronson C, McCall W R, Chen S and Sirbuly D J 2014 3D optical printing of piezoelectric nanoparticle–polymer composite materials *ACS nano* **8** 9799-806

[9] Li J Y 2000 The effective electroelastic moduli of textured piezoelectric polycrystalline aggregates *Journal of the Mechanics and Physics of Solids* **48** 529-52

[10] Zheng P, Zhang J, Tan Y and Wang C 2012 Grain-size effects on dielectric and piezoelectric properties of poled BaTiO3 ceramics *Acta Materialia* **60** 5022-30

[11] Jagdish A K, Buroni F C, Garcia-Sanchez F, Melnik R V N, Rodriguez-Tembleque L and Sáez A 2019 Improving the performance of lead-free piezoelectric composites by using polycrystalline inclusions and tuning the dielectric matrix environment (Submitted)

[12] Hikita K, Yamada K, Nishioka M and Ono M 1983 Piezoelectric properties of the porous PZT and the porous PZT composite with silicone rubber *Ferroelectrics* **49** 265-72

[13] Ibn-Mohammed T, Koh S, Reaney I, Sinclair D, Mustapha K, Acquaye A and Wang D 2017 Are lead-free piezoelectrics more environmentally friendly? *MRS Communications* **7** 1-7

[14] Dudem B, Kim D H, Bharat L K and Yu J S 2018 Highly-flexible piezoelectric nanogenerators with silver nanowires and barium titanate embedded composite films for mechanical energy harvesting *Applied Energy* **230** 865-74

[15] Shi K, Huang X, Sun B, Wu Z, He J and Jiang P 2019 Cellulose/BaTiO3 aerogel paper based flexible piezoelectric nanogenerators and the electric coupling with triboelectricity *Nano Energy* **57** 450-8

[16] He X, Wang D, Wang L and Melnik R V N 2018 Modelling of creep hysteresis in ferroelectrics *Philosophical Magazine* **98** 1256-71

[17] Prabhakar S, Melnik R V N, Neittaanmäki P and Tiihonen T 2013 Coupled magneto-thermo-electromechanical effects and electronic properties of quantum dots *Journal of Computational and Theoretical Nanoscience* **10** 534-47

[18] Wang D, Du H, Wang L and Melnik R V N 2018 A phase field approach for the fully coupled thermo-electro-mechanical dynamics of nanoscale ferroelectric actuators *Smart Materials and Structures* **27** 055012

[19] Wang D, Melnik R V N and Wang L 2018 Material influence in newly proposed ferroelectric energy harvesters *Journal of Intelligent Material Systems and Structures* **29** 3305-16

[20] Wang D, Wang L and Melnik R V N 2017 Vibration energy harvesting based on stress-induced polarization switching: a phase field approach *Smart Materials and Structures* **26** 065022

[21] Sriphan S, Nawanil C and Vittayakorn N 2018 Influence of dispersed phase morphology on electrical and fatigue properties of BaTiO3/PDMS nanogenerator *Ceramics International* **44** S38-S42

[22] Zhang Y, Sun H and Jeong C K 2018 Biomimetic Porifera Skeletal Structure of Lead-Free Piezocomposite Energy Harvesters *ACS applied materials & interfaces* **10** 35539-46

[23] Baek C, Yun J H, Wang H S, Wang J E, Park H, Park K-I and Kim D K 2018 Enhanced output performance of a lead-free nanocomposite generator using BaTiO3 nanoparticles and nanowires filler *Applied Surface Science* **429** 164-70

[24] Sun Y, Chang Y, Wu J, Liu Y, Jin L, Zhang S, Yang B and Cao W 2019 Ultrahigh energy harvesting properties in textured lead-free piezoelectric composites *Journal of Materials Chemistry A*

[25] Kim H, Torres F, Islam M T, Islam M D, Chavez L A, Garcia Rosales C A, Wilburn B R, Stewart C M, Noveron J C, Tseng T-L B and Lin Y 2017 Increased piezoelectric response in functional nanocomposites through multiwall carbon nanotube interface and fused-deposition modeling three-dimensional printing *MRS Communications* **7** 960-6

[26] Fan B, Liu Y, He D and Bai J 2018 Achieving polydimethylsiloxane/carbon nanotube (PDMS/CNT) composites with extremely low dielectric loss and adjustable dielectric constant by sandwich structure *Applied Physics Letters* **112** 052902

[27] Li J, Ma P C, Chow W S, To C K, Tang B Z and Kim J K 2007 Correlations between percolation threshold, dispersion state, and aspect ratio of carbon nanotubes *Advanced Functional Materials* **17** 3207-15

[28] Sandler J, Kirk J, Kinloch I, Shaffer M and Windle A 2003 Ultra-low electrical percolation threshold in carbon-nanotube-epoxy composites *Polymer* **44** 5893-9

[29] Martone A, Faiella G, Antonucci V, Giordano M and Zarrelli M 2011 The effect of the aspect ratio of carbon nanotubes on their effective reinforcement modulus in an epoxy matrix *Composites Science and Technology* **71** 1117-23

[30] Bao H-D, Sun Y, Xiong Z-Y, Guo Z-X and Yu J 2013 Effects of the dispersion state and aspect ratio of carbon nanotubes on their electrical percolation threshold in a polymer *Journal of Applied Polymer Science* **128** 735-40

[31] Tarlton T, Sullivan E, Brown J and Derosa P A 2017 The role of agglomeration in the conductivity of carbon nanotube composites near percolation *Journal of Applied Physics* **121** 085103

[32] Kundalwal S and Choyal V 2018 Transversely isotropic elastic properties of carbon nanotubes containing vacancy defects using MD *Acta Mechanica* 1-14

[33] Bao H-D, Guo Z-X and Yu J 2008 Effect of electrically inert particulate filler on electrical resistivity of polymer/multi-walled carbon nanotube composites *Polymer* **49** 3826-31

[34] Saputra A A, Sladek V, Sladek J and Song C 2018 Micromechanics determination of effective material coefficients of cement-based piezoelectric ceramic composites *Journal of Intelligent Material Systems and Structures* **29** 845-62

[35] Melnik R V N 2000 Generalised solutions, discrete models and energy estimates for a 2D problem of coupled field theory *Applied Mathematics and Computation* **107** 27-55

[36] Melnik R V N 2003 Computationally efficient algorithms for modelling thermal degradation and spiking phenomena in polymeric materials *Computers & Chemical Engineering* **27** 1473-84

[37] Bai L, Li Z, Zhao S and Zheng J 2018 Covalent functionalization of carbon nanotubes with hydroxyl-terminated polydimethylsiloxane to enhance filler dispersion, interfacial adhesion and performance of poly (methylphenylsiloxane) composites *Composites Science and Technology* **165** 274-81

[38] Lewicki J P, Liggat J J and Patel M 2009 The thermal degradation behaviour of polydimethylsiloxane/montmorillonite nanocomposites *Polymer Degradation and Stability* **94** 1548-57

[39] Norkhairunnisa M, Azizan A, Mariatti M, Ismail H and Sim L 2012 Thermal stability and electrical behavior of polydimethylsiloxane nanocomposites with carbon nanotubes and carbon black fillers *Journal of Composite Materials* **46** 903-10

[40] Johnston I, McCluskey D, Tan C and Tracey M 2014 Mechanical characterization of bulk Sylgard 184 for microfluidics and microengineering *Journal of Micromechanics and Microengineering* **24** 035017

[41] Shen L and Li J 2005 Transversely isotropic elastic properties of multiwalled carbon nanotubes *Physical Review B* **71** 035412

[42] Rodríguez-Tembleque L, García-Macías E and Sáez A 2018 CNT-polymer nanocomposites under frictional contact conditions *Composites Part B: Engineering* **154** 114-27

[43] Shi D-L, Feng X-Q, Huang Y Y, Hwang K-C and Gao H 2004 The effect of nanotube waviness and agglomeration on the elastic property of carbon nanotube-reinforced composites *Journal of Engineering Materials and Technology* **126** 250-7

[44] Pecharroman C, Esteban-Betegon F, Bartolome J F, Lopez-Esteban S and Moya J S 2001 New Percolative BaTiO3–Ni Composites with a High and Frequency-Independent Dielectric Constant (ϵr≈ 80000) *Advanced Materials* **13** 1541-4

[45] Vaisman L, Wagner H D and Marom G 2006 The role of surfactants in dispersion of carbon nanotubes *Advances in Colloid and Interface Science* **128-130** 37-46

[46] Li Q, Xue Q, Hao L, Gao X and Zheng Q 2008 Large dielectric constant of the chemically functionalized carbon nanotube/polymer composites *Composites Science and Technology* **68** 2290-6

[47] Wang F, Wang J-W, Li S-q and Xiao J 2009 Dielectric properties of epoxy composites with modified multiwalled carbon nanotubes *Polymer bulletin* **63** 101-10

[48] Tao H and Wu J 2017 New poling method for piezoelectric ceramics *Journal of Materials Chemistry C* **5** 1601-6

[49] Melnik R V N, Uhlherr A, Hodgkin J and De Hoog F 2003 Distance geometry algorithms in molecular modelling of polymer and composite systems *Computers & Mathematics with Applications* **45** 515-34

[50] Aghadavoudi F, Golestanian H and Tadi Beni Y 2018 Investigating the effects of CNT aspect ratio and agglomeration on elastic constants of crosslinked polymer nanocomposite using multiscale modeling *Polymer Composites* **39** 4513-23
[51] Alian A R and Meguid S 2018 Large-scale atomistic simulations of CNT-reinforced thermoplastic polymers *Composite Structures* **191** 221-30
[52] Ghajar R, Shokrieh M M and Shajari A R 2018 An experimental investigation on the viscoelastic properties of CNT reinforced CY 219 epoxy resin, using DMTA and creep tests *Materials Research Express* **5** 085033
[53] Chen S J, Qiu C Y, Korayem A H, Barati M R and Duan W H 2016 Agglomeration process of surfactant-dispersed carbon nanotubes in unstable dispersion: A two-stage agglomeration model and experimental evidence *Powder Technology* **301** 412-20
[54] Choi H K, Jung H, Yu J and Shin E S 2015 Prediction of Thermo-mechanical Behavior for CNT/epoxy Composites Using Molecular Dynamics Simulation *Composites Research* **28** 260-4

Figures (main text)

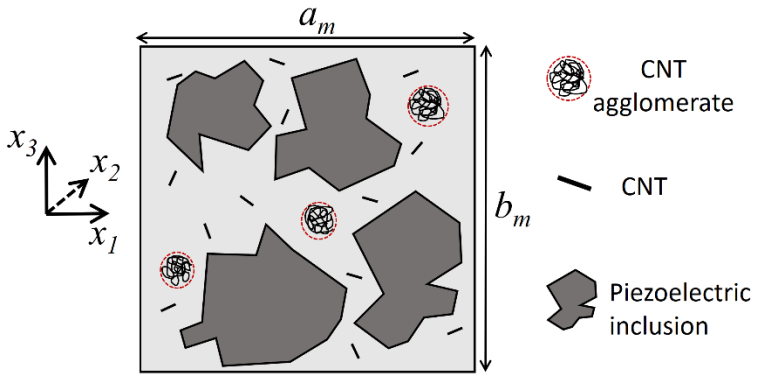

Figure 1 – Schematic of the piezoelectric composite RVE with randomly shaped polycrystalline piezoelectric inclusions randomly dispersed in a square matrix. The matrix is further modified by the addition of carbon nanotubes (multiwalled or single-walled) and is assumed to contain agglomerates of these nanotubes. The axis system used in the study is also illustrated.

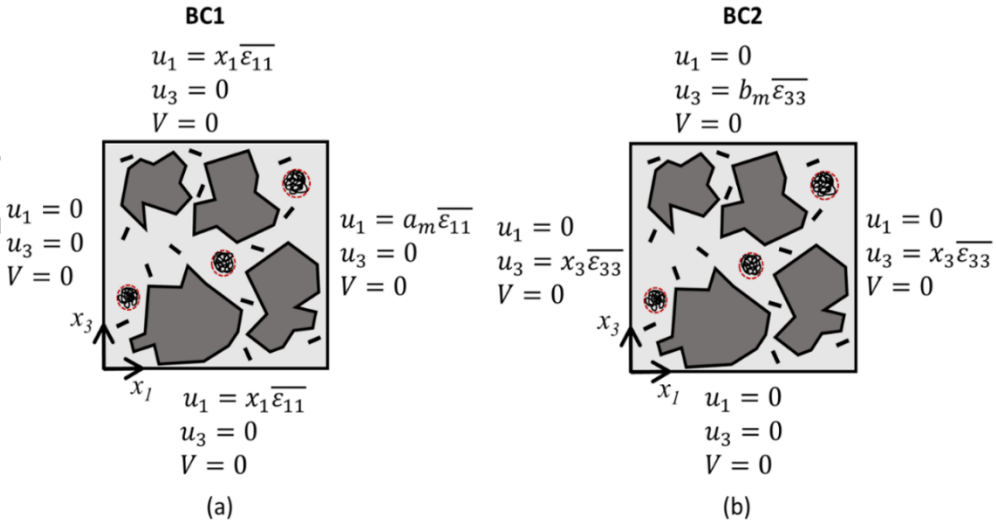

Figure 2 – Two sets of boundary conditions (a) BC1 and (b) BC2, used to calculate the effective electro-elastic coefficients of the composite.

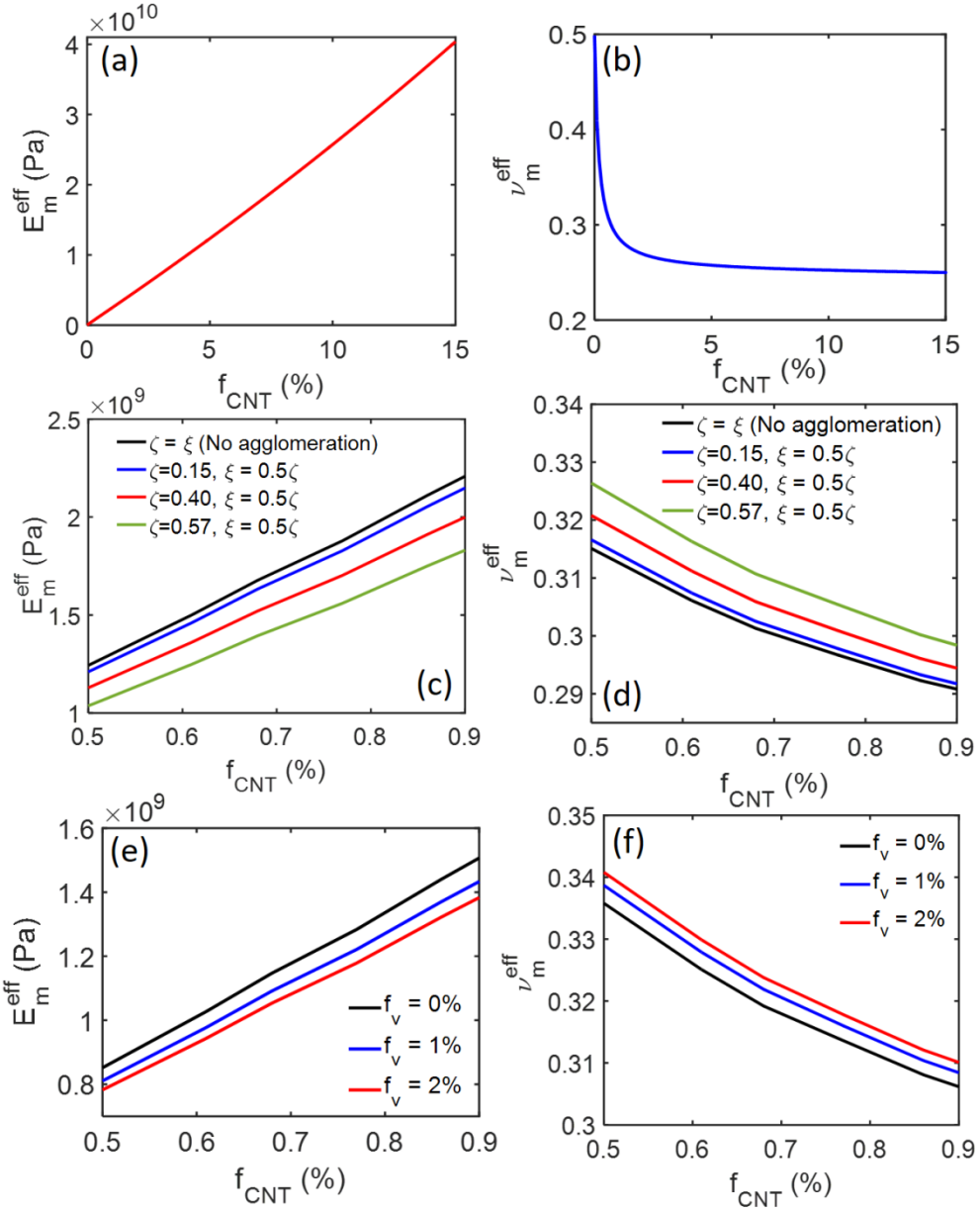

Figure 3 (color online) – The effective Young's modulus E_m^{eff} and the effective Poisson' ratio ν_m^{eff} of the PDMS matrix as a function of the MWCNT fill fraction f_{CNT},(a)-(b) plot the effective parameters for a system without nanotube agglomerations, (c)-(d) plot the effective parameters for agglomerated systems.

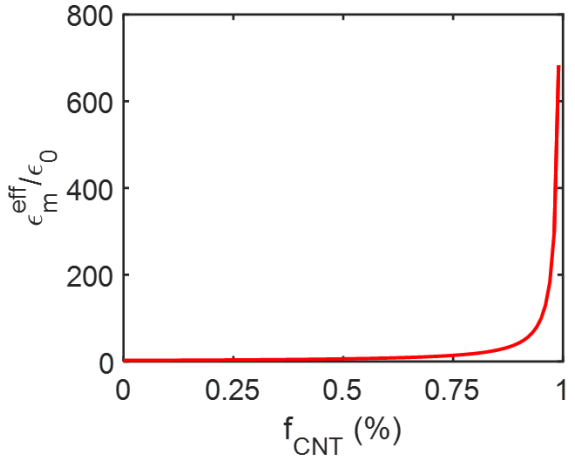

Figure 4 – The percolative dependence of the relative permittivity of the matrix on the carbon nanotube fill-fraction f_{CNT}. Here, the percolation threshold, f_c, and the critical exponent, p, are assumed to be 1% and 1.2 respectively.

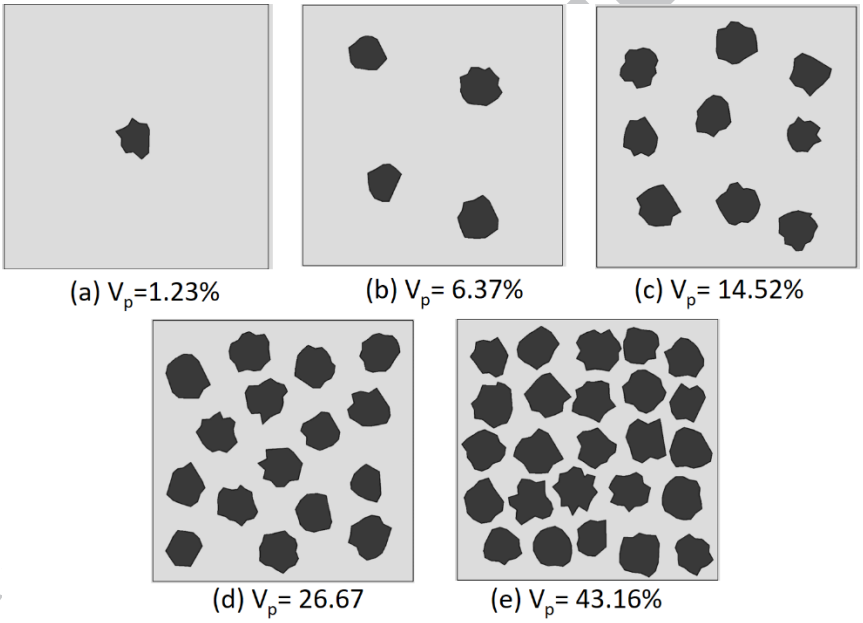

Figure 5 – The five RVEs considered in this study along with different piezoelectric inclusion fill fractions V_p.

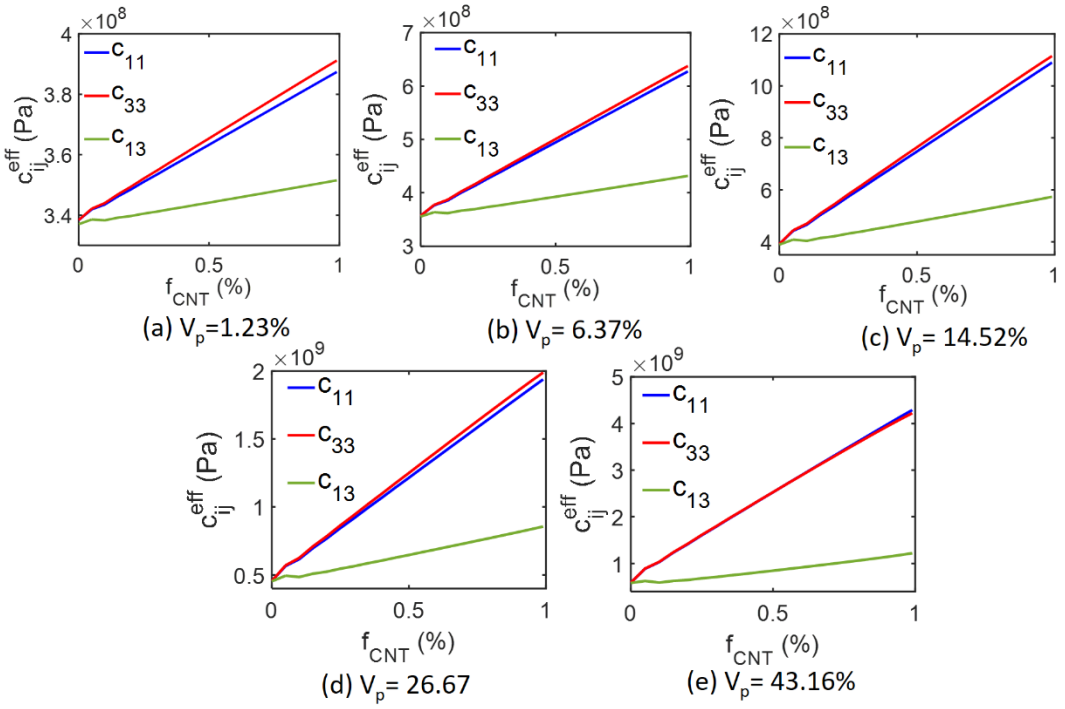

Figure 6 (color online) – The effective elastic moduli of the composites with uniformly dispersed nanotubes, as a function of the nanotube fill-fraction f_{CNT}. (a)-(e) show relations between the effective moduli and f_{CNT} for various piezoelectric inclusion fill fractions V_p. α=0 in all these plots.

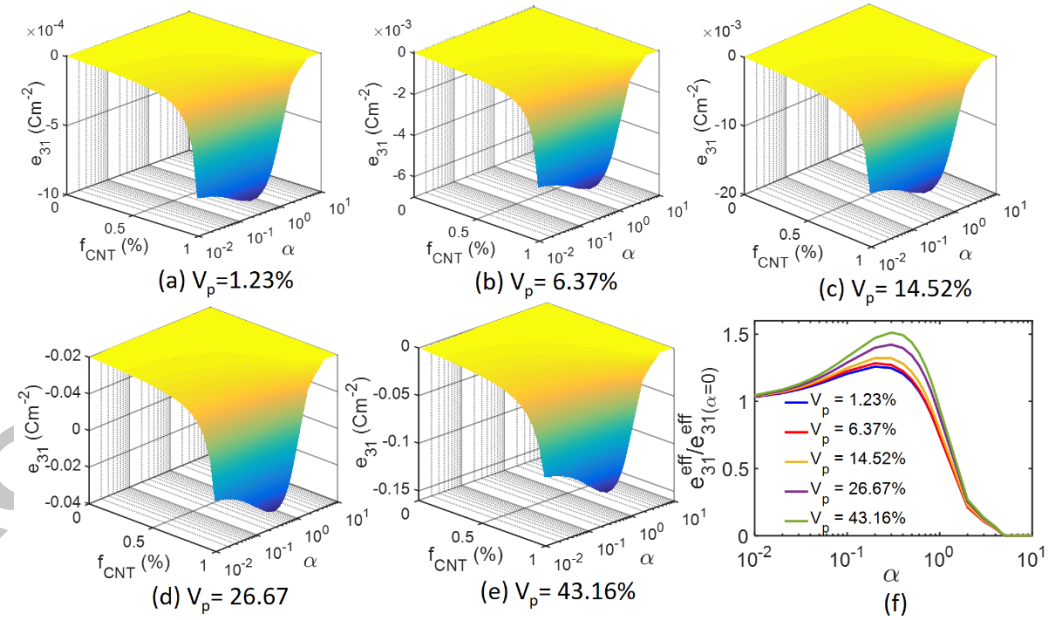

Figure 7 – The effective coefficient e_{31} of the composite as a function of the polycrystalline orientation parameter, α, and nanotube fill-fraction f_{CNT}, shown for different volume fractions V_p of the piezoelectric inclusions in (a)-(e). (f) shows the effective parameter e_{31} (color online) as a function of α, relative to its value at α=0, near the percolation threshold for the nanotubes (i.e. f_{CNT}=0.99%, where f_c=1.0%).

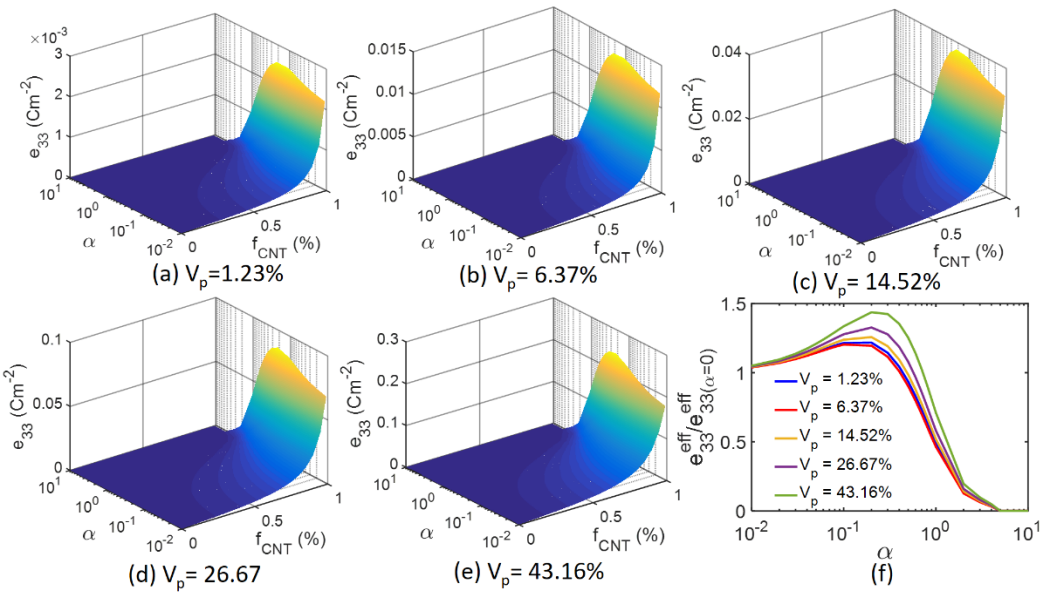

Figure 8– The effective coefficient e_{31} of the composite as a function of the polycrystalline orientation parameter α, and nanotube fill-fraction f_{CNT}, shown for different volume fractions V_p of the piezoelectric inclusions in (a)-(e). (f) shows the effective parameter e_{31} (color online) as a function of α, relative to its value at α=0, near the percolation threshold for the nanotubes (i.e. f_{CNT}=0.99%, where f_c=1.0%).

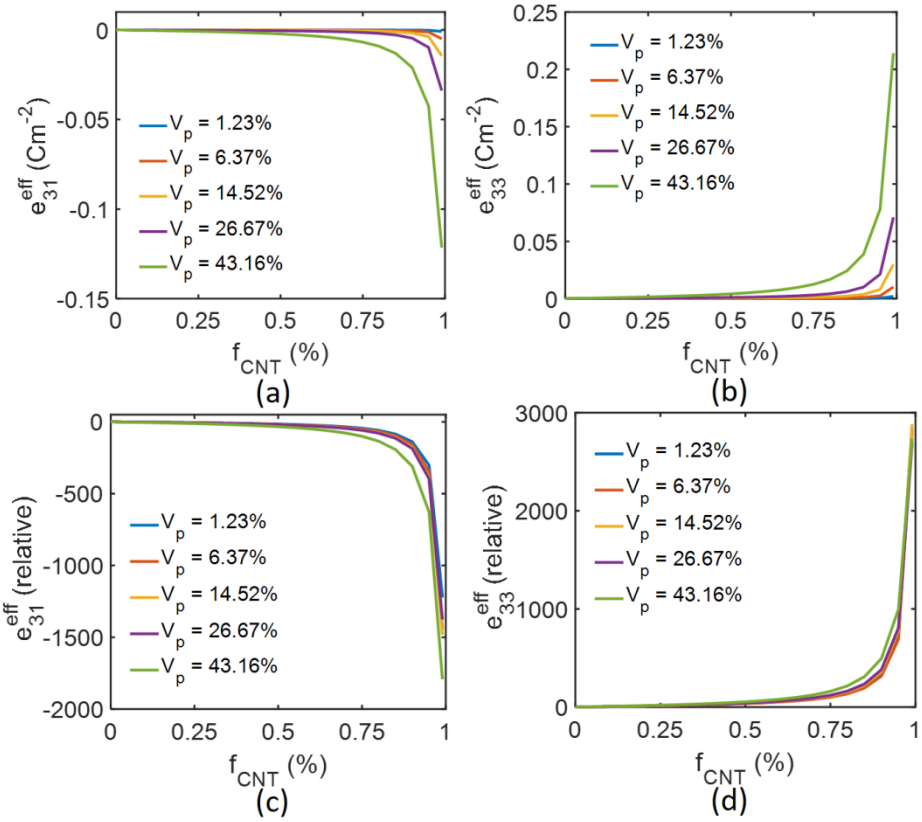

Figure 9 (color online) – (a) and (b) show the effective parameters e_{31} and e_{33} of composites as a function of the nanotube fill fraction f_{CNT}, for different volume fractions V_p of the piezoelectric inclusions. (c) and (d) show the same effective parameters as (a) and (b), respectively, relative to their values with pristine matrices without CNT addition.

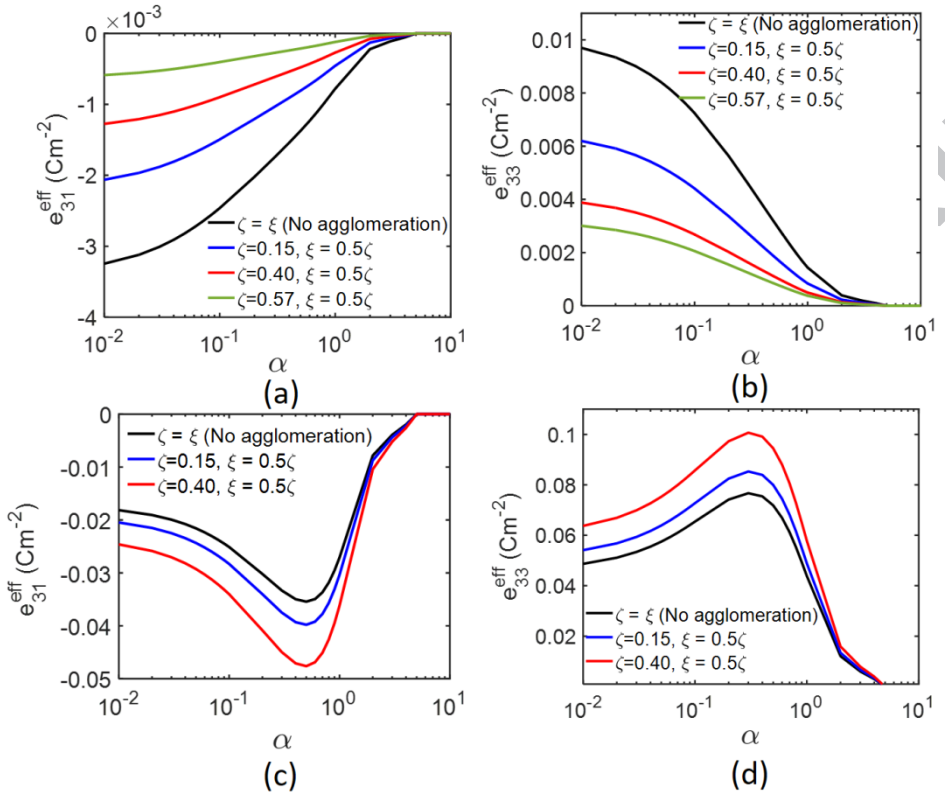

Figure 10 (color online)– (a) and (b) show the effective coefficients e_{31} and e_{33} respectively, for various states of nanotube agglomeration, with f_{CNT}=0.5%, (c) and (d) show the effective coefficients e_{31} and e_{33} of the composite, for various states of agglomeration with f_{CNT}=0.999f_c.

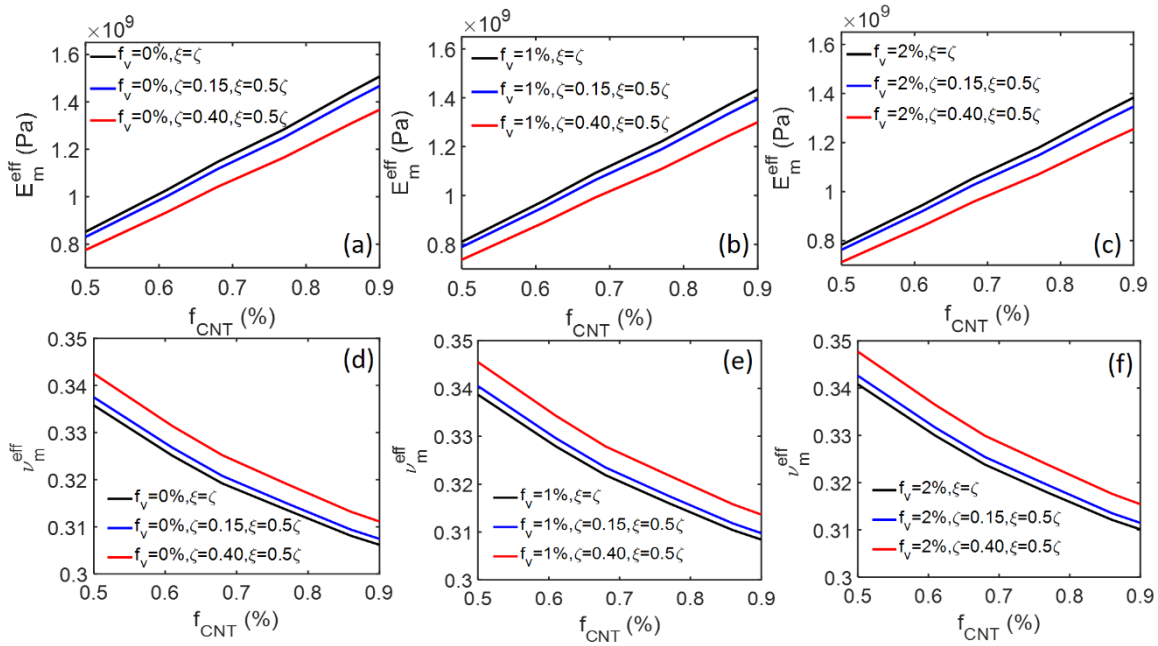

Figure 11 (color online) – The effective elastic properties of the PDMS matrix modified by (15,15) SWCNTs with simultaneous presence of atomic vacancy defects and nanotube agglomerations. The results are plotted for vacancy concentration f_v = 0%,1%, and 2%.

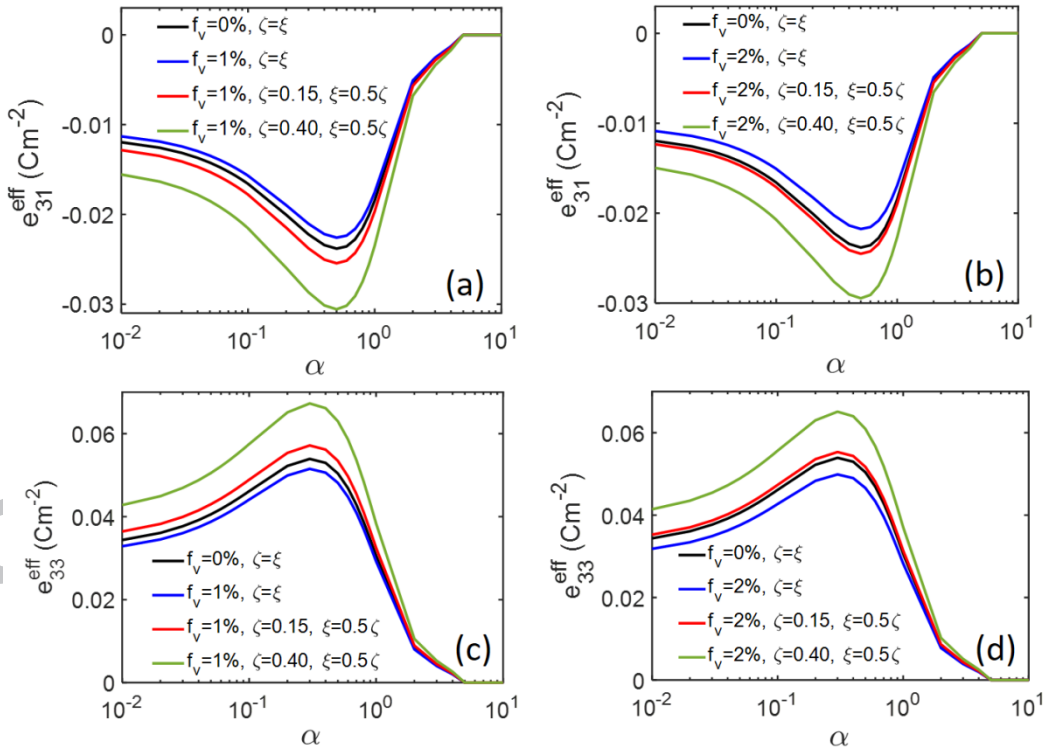

Figure 12 (color online) – The effective coefficients e_{31} ((a)-(b)) and e_{33} ((c)-(d)) of composites SWCNTs with atomic vacancies and nanotube agglomerations. The reference sample has f_v=0 and no agglomerations (i.e. $\zeta = \xi$). (a) and (c) compare the results with f_v=1% and increasing agglomeration, and (b) and (d) compare the results with f_v=2% and increasing agglomerations.

Figures (appendices)

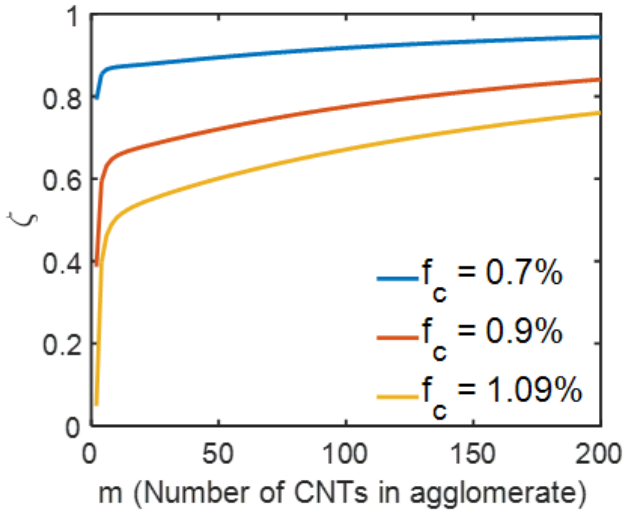

Figure AF1 – The agglomeration state ζ as a function of number of CNTs, m, in an agglomerate.

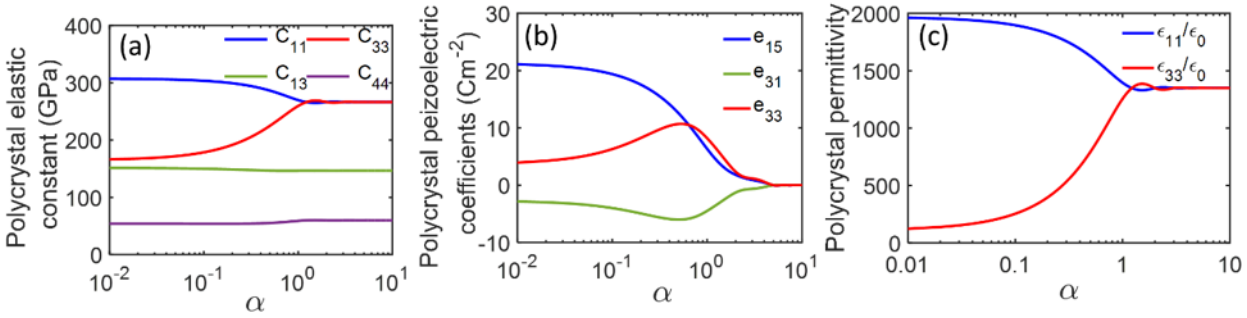

Figure AF2 – Effective electro-elastic coefficients of polycrytalline $BaTiO_3$ as a function the orientation parameter α.

Tables

Table 1 – Geometrical parameters exemplified in the simulations.

Matrix		
Geometrical parameter		**Value (μm)**
a_m		150
b_m		150
Inclusions (Radially bound between two concentric circles of random radii R_1 and R_2)		
Geometric parameter		**Value (μm)**
R_1 range		7.5-10.5
R_2 range		12.0-15.0
Carbon nanotubes		
Type	**$2R_{CNT}$ (nm)**	**$\lambda=L_{CNT}/2R_{CNT}$**
SWCNT (15,15)	2.04	100
MWCNT (15,15)	2.04	100

Table 2- Mechanical and dielectric properties of the matrix materials used in this study.

Material constant	**M1: PDMS (soft matrix) [40]**
Tensile modulus, E_m (Pa)	2×10^6
Poisson's ratio, v_m	0.499
ϵ_{11}/ϵ_0	2.72
ϵ_{33}/ϵ_0	2.72

Table 3: The agglomeration states and the corresponding percolation thresholds considered in this study.

f_c (%)	0.7	0.9	1.09
ζ	0.15	0.40	0.57